

10. EARLY OLIGOCENE–PLEISTOCENE CALCAREOUS NANNOFOSSIL BIOSTRATIGRAPHY OF THE NORTHERN SOUTH CHINA SEA (LEG 184, SITES 1146–1148)¹

Xin Su,² Yulin Xu,² and Quiang Tu²

ABSTRACT

Sites 1146 and 1148 of Ocean Drilling Program Leg 184, in the South China Sea (SCS), comprise long sediment sections with a time span from the early Oligocene to the Pleistocene. Calcareous nannofossils from these two sites were biostratigraphically studied.

We recognized 53 early Oligocene to Pleistocene events that are commonly found in open sea areas and can therefore be correlated within a large geographic range. This study also revealed that a few conventionally used nannofossil events are not suitable for the SCS, and further evaluation is needed.

The lower Oligocene to Pleistocene sequences recovered at Sites 1146 and 1148 were subdivided into the 4 Paleogene zones and 21 Neogene to Quaternary zones of Martini, in correlation with the Paleogene to Quaternary zones of Okada and Bukry. This provided a lower Oligocene through Pleistocene nannofossil biostratigraphic framework.

A significant unconformity was recognized in the Oligocene–Miocene transition, in which the upper part of Oligocene Zone NP25 and lower part of Miocene Zone NN1 were missing. The time span of the unconformity was estimated to be ~1 m.y.

Very high sedimentation rates were seen in the Oligocene, relative low values were seen in the Miocene, and the highest values were seen in the Pleistocene, which was believed to be the result of tectonic and sedimentation history of the SCS.

¹Su, X., Xu, Y., and Tu, Q., 2004. Early Oligocene–Pleistocene calcareous nannofossil biostratigraphy of the northern South China Sea (Leg 184, Sites 1146–1148). *In* Prell, W.L., Wang, P., Blum, P., Rea, D.K., and Clemens, S.C. (Eds.), *Proc. ODP, Sci. Results*, 184, 1–24 [Online]. Available from World Wide Web: <http://www-odp.tamu.edu/publications/184_SR/VOLUME/CHAPTERS/224.PDF>.

[Cited YYYY-MM-DD]

²China University of Geosciences (Beijing), Xueyuan Road 29, Beijing, 100083, People's Republic of China. xsu@cugb.edu.cn

Initial receipt: 30 January 2004

Acceptance: 9 August 2004

Web publication: 19 November 2004

Ms 184SR-224

INTRODUCTION

The South China Sea (SCS) is the largest marginal sea in the West Pacific. Previous biostratigraphic studies on calcareous nannofossils in the SCS were limited to incomplete Oligocene to Pleistocene marine sequences from exploration wells in offshore basins (Duan and Huang, 1991; Huang and Zhong, 1992; Xu, 1996; Huang, 1997) or late Quaternary materials from shallow piston cores in the deep-sea area (Duan, 1985; Su, 1989).

During Ocean Drilling Program (ODP) Leg 184 (Fremantle to Hong Kong, February–April 1999), the *JOIDES Resolution* drilled six sites in the deep-sea area of the SCS. This was the first time that sediment cores deeper than 20 m were sampled from the continental slope in the SCS. Of these six sites, Sites 1146 and 1148 were the source of the two longest sections from the SCS: a 642-m-long composite section spanning the last 18 m.y. at Site 1146 and an 861-m-long composite section spanning the last 32 m.y. from Sites 1147 and 1148. Sediments recovered at these two sites yield abundant and well-preserved calcareous nannofossils.

The objective of this study was to establish an early Oligocene to Pleistocene calcareous nannofossil biostratigraphic framework for the northern SCS.

MATERIAL AND METHODS

Materials

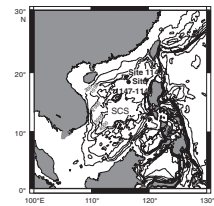
Sites and Samples

Early Oligocene to Pleistocene calcareous nannofossils at Sites 1146, 1147, and 1148 in the northern SCS (Fig. F1; Table T1) were analyzed. Sample spacing is ~100 cm for Site 1146 and 150 cm for Sites 1147 and 1148. A total of 1200 samples were examined.

Site 1146 is located at a water depth of 2092 m within a small rift basin on the mid-continental slope of the northern SCS (Fig. F1). Coring at Site 1146 recovered a 600-m-long, lower Miocene through Pleistocene section of relatively carbonate rich, hemipelagic nannofossil clays with a basal age of ~19 Ma. Site 1146 provides one of the most continuous Neogene sections ever recovered by ODP. Sediments recovered at Site 1146 yield abundant nannofossils that are generally well preserved above 531.2 mcd but are moderately overgrown below that level. Many samples exhibited some degree of reworking. For this reason, a number of last occurrence (LO) events at this site were determined based on semiquantitative methods.

Site 1148 is located at a water depth of ~3294 m on the lowermost continental slope off southern China near the continent/ocean crust boundary and is the most offshore site drilled during Leg 184 (Fig. F1). Site 1147 is located at a water depth of ~3245 m ~0.45 nmi upslope from Site 1148 (Fig. F1) and was designed to recover the uppermost section that appeared to be missing on seismic profiles from Site 1148 (Wang, Prell, Blum, et al., 2000). Sediments at Site 148 yielded abundant nannofossils with preservation that varied downhole. Reworked nannofossils are commonly seen at this site, particularly in early Miocene to late Oligocene Cores 184-1148A-44X, 48X, and 49X. Pro-

F1. Location of ODP Sites 1146, 1147, and 1148, p. 15.



T1. Location of Sites 1146, 1147, and 1148, p. 22.

Ages of Cenozoic chronostratigraphic boundaries were established by Berggren et al. (1995). According to this study, the age of the Oligocene/Miocene boundary is 23.80 Ma, the age of the Miocene/Pliocene boundary is 5.32 Ma, and that of the Pliocene/Pleistocene boundary is 1.77 Ma, as given in Figure F2.

Taxonomic Remarks

Identification of most calcareous nannofossils primarily follows the compilation of Perch-Nielsen (1985). Only a few of species are discussed here.

Gephyrocapsa

Several *Gephyrocapsa* species are commonly used as biostratigraphic markers. However, morphologic intergradations exist between species, leading to confusion in identification (Su, 1996). A detailed study is needed to find reliable and applicable criteria to separate them. Thus, only one morphological group, *Gephyrocapsa* (medium) spp., which is relatively easy to identify, was used in this study. This group includes very early Pleistocene forms of *Gephyrocapsa magereli* and *Gephyrocapsa lumina*, and their variants, with a maximum coccolith length $>3.5\ \mu\text{m}$.

Reticulofenestra

A number of *Reticulofenestra* species—*Reticulofenestra asanoi*, *Reticulofenestra pseudoumbilicus*, and *Reticulofenestra umbilicus*, for example—have been used as Tertiary and Quaternary biostratigraphic markers. They are mostly distinguished by coccolith size (cutoff size), showing a great range of variation in these parameters and causing problems in identification (Backman, 1980; Gallagher, 1989; Young, 1990; Su, 1996). To ensure taxonomic consistency with previous work, we followed the commonly accepted cutoff sizes: the coccolith length of *R. asanoi* is $>5\ \mu\text{m}$ (Sato and Takayama, 1992), and that of *R. pseudoumbilicus* is $>7\ \mu\text{m}$, in accord with the size of the holotype (Gartner, 1967). Typical *R. umbilicus* can be easily distinguished from other species by its enormous size. However, morphological intergradations exist between this species and other smaller forms, such as *Reticulofenestra dictyoda* or *Reticulofenestra coenura*. Backman and Hermelin (1986) suggested using a lower size limit of $14\ \mu\text{m}$ for recognition of *R. umbilicus*, and this suggestion has been widely accepted. *Reticulofenestra hillae*, a large elliptical form, has been considered as an eco-phenotype or a variety of *R. umbilicus* (Backman and Hermelin, 1986; Berggren et al., 1995). In agreement with these studies, we combined *R. umbilicus* and *R. hillae* as a group named *R. umbilicus* with a cutoff size of $14\ \mu\text{m}$.

Sphenolithus

In this study, a number of *Sphenolithus* species or taxa were employed following Perch-Nielsen (1985). Only the separation of a group of morphologically and phylogenetically related species, *Sphenolithus predistentus*-*Sphenolithus ciperoensis* lineage, followed Moran and Watkins (1988). Okada (1990) further observed morphological variances of *S. ciperoensis* and *Sphenolithus distentus* from the tropical and subtropical Indian Ocean and named them *Sphenolithus* aff. *ciperoensis* and *Sphenolithus* aff. *distentus*. *Sphenolithus* aff. *ciperoensis* resembles *S. ciperoensis*, but the apical spine is shorter and wider than the type species. Furthermore, the basal spines of the former are thinner and arranged to form a more widely spread base than the latter. Okada (1990) also found that the V-shaped basal line of *Sphenolithus* aff. *distentus* is similar to the typ-

ical *S. distentus*, but the apical spine and overall size of the former is larger (7–12 μm compared to $\sim 5 \mu\text{m}$). *Sphenolithus* aff. *ciperoensis* and *Sphenolithus* aff. *distentus* are also present in our Oligocene materials, hampering identification and determination of the FO of *S. ciperoensis* and *S. distentus*. To separate these variants, we followed the criteria suggested by Okada (1990).

RESULTS

Biostratigraphy

A total of 53 nannofossil events were recognized in the lower Oligocene to Pleistocene sediments studied (Tables T2, T3). This allows the subdivision of four upper Paleogene zones of Martini (1971) and his 21 Neogene to Quaternary zones or three late Paleogene zones of Okada and Bukry (1980) and their Neogene to Quaternary 15 zones (Fig. F3). A brief description of the result is given here with focus on biostratigraphic problems that occurred and solutions used during this study.

Oligocene

Upper Oligocene sediments were only recovered from Site 1148. The LO of *Emiliana formosa* marks the NP21/NP22 or CP16b/CP16c zonal boundaries. This event was also useful for defining the NP21/NP22 zonal boundary in adjacent areas of the SCS, such as in the Celebes Sea (Shyu and Müller, 1991) and in the West Philippine Sea (Shipboard Scientific Party, 2002). At Site 1148, only one specimen of *E. formosa* was observed at a depth of 671.89 mcd, above the FO of *S. distentus*. This specimen is clearly a reworked fossil. *E. formosa* is actually absent in the 851.4-m-long sequence at Site 1148, suggesting that Site 1148 does not penetrate through the NP21/NP22 zonal boundary and the sediments at the base of Site 1148 are still in the lowermost lower Oligocene Zone NP22 with an age of younger than 32.8 Ma.

In our materials, we did not observe typical *R. umbilicus* but found $>14\text{-}\mu\text{m}$ -sized *R. hillae*. This allowed us to recognize the LO of *R. umbilicus* at 730.33 mcd at Site 1148. It is the earliest event at this site and serves as the marker for the NP22/NP23 boundary and assigns the interval below it to Zone NN22 or to Subzone CP16c (Table T3; Fig. F3).

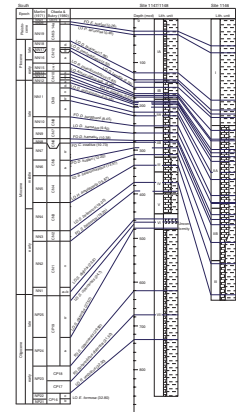
In many open-ocean areas, for example in the Southern Ocean, the LO of *Isthmolithus recurvus* appears between the LO of *R. umbilicus* and the LO of *E. formosa* (Poore et al., 1982; Wei and Thierstein, 1991). This species is absent in our materials. It is also absent in the Eocene to the lower Oligocene sediments at Site 1201 in the West Philippine Sea (Shipboard Scientific Party, 2002). All of these imply that *I. recurvus* might be absent or rare in the low Pacific latitudes, supporting Wei (1992), who suggested that the FO and LO of *I. recurvus* are only applicable in the mid and high latitudes but not useful in low latitudes.

The FO of *S. ciperoensis* at Site 1148 was determined by separating typical *S. ciperoensis* from *Sphenolithus* aff. *ciperoensis*, using the method of Okada (1990). As a result, the FO of true *S. ciperoensis* was placed at depth 617.16 mcd and the FO of *S. distentus* was placed at 671.89 mcd (Table T2). In our materials studied, however, *Sphenolithus* aff. *ciperoensis* appears sporadically down to 655.52 mcd, much lower than the level of the FO of true *S. ciperoensis*, and differing from the case of ODP Leg

T2. Depths and ages of calcareous nannofossil events, Site 1148, p. 23.

T3. Depths and ages of calcareous nannofossil events, Site 1146, p. 24.

F3. Correlation of calcareous nannofossil zones, p. 18.



115, where *S. ciproensis* and *Sphenolithus* aff. *ciproensis* show the same stratigraphic range (Backman et al., 1990).

The next event, the LO of *S. distentus*, was determined at the depth of 477.34 mcd, marking the NP24/NP25 zonal boundary. Trace *S. distentus* was found occasionally; for example, it appears in a few samples of Core 184-1148A-48X, where redeposited carbonate mud clasts or layers were observed (Wang, Prell, Blum, et al., 2000). Therefore, we considered the trace occurrence of this species in that core as reworked. The near absence of *S. distentus* in Core 184-1148-49X, where several slumping layers are present (Wang, Prell, Blum, et al., 2000), indicates slumping occurred after the LO of *S. distentus* (27.5 Ma), or above Zone NP24. *S. predistentus* disappears with *S. distentus* together in the same sample at Site 1148 (Table T2).

Oligocene–Miocene Transition

The most difficult work at Site 1148 is to surely determine the events in Cores 184-1148A-47X and 48X, the upper Oligocene to lower Miocene interval. The problems were how to determine a number of late Oligocene LO events from sediments dominated by reworking, faulting, and slumping and to identify early Miocene events from poorly preserved fossils.

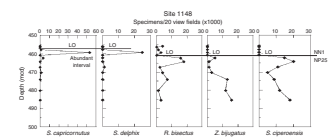
Sample 184-1148A-48X-6, 80–81 cm (462.32 mcd), contains common to few upper Oligocene *Reticulofenestra bisectus*, *Zygrhhablithus bijugatus*, *S. ciproensis*, and *Chiasmolithus altus* (Figs. F4, F5). In a normal sediment sequence, the sequence of the LOs of these species should appear as follows: *R. bisectus* (23.9 Ma), *Z. bijugatus* (24.5 Ma), *S. ciproensis* (24.75 Ma), and *C. altus* (26.1 Ma). The appearance of these LOs in the same sample suggests that we did not see the real LOs of these species; the uppermost ranges of *R. bisectus*, *Z. bijugatus*, and *S. ciproensis*, and, possibly, the uppermost range of *C. altus*, are truncated. In the same core, we observed abundant *Sphenolithus capricornutus* and *Sphenolithus delphix* in Sample 184-1148-48X-4, 81–82 cm, where rare *R. bisectus*, *Z. bijugatus*, and *S. ciproensis* also appear (458.57 mcd) (Table T2; Figs. F4, F5).

Based on semiquantitative observations (Fig. F4), we took the common occurrence of *S. ciproensis* as its LO (24.75 Ma) in Sample 184-1148A-48X-6, 80–81 cm (462.32 mcd). Its sporadic and few presence in the samples above was considered as reworking. Abundant *S. capricornutus* and *S. delphix* in Sample 184-1148-48X-4, 81–82 cm, were determined as their LOs (23.7 and 23.8 Ma, respectively). In this case, the presence of few *R. bisectus* and *Z. bijugatus* above 462.32 mcd was also considered to be due to reworking. Consequently, the LOs of *R. bisectus* and *Z. bijugatus* were not seen and their uppermost ranges were truncated. As for *C. altus*, it appears very sporadically in upper Oligocene sediments; we were unable to determine if its LO in this interval is caused by reworking, and therefore we did not use it for further discussion.

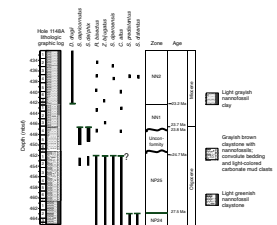
For defining the NP25/NN1 and the CP19b/CN1a zonal boundaries, we still followed Berggren et al. (1995), who used the LO of *R. bisectus* (23.9 Ma). The determination of the LO of *S. ciproensis* and the truncation of the uppermost range of *R. bisectus* at Site 1148 suggests that the uppermost range of Zone NP25 was truncated as well, but its upper part exists at Site 1248 (Fig. F5).

Rio et al. (1990) found a short acme interval of *S. delphix* with *S. capricornutus* slightly below the FO of *Discoaster druggii* in the subtropic and

F4. Variation in abundance of several marker species, p. 19.



F5. Appearance of several marker species, p. 20.



tropic Indian Ocean, and these two species are virtually restricted to the upper part of Zone NN1 (Subzone CN1c). An abundant *S. delphix* interval between the LO of *S. ciproensis* and the FO of *D. druggii* is also present in ODP Hole 807A from the Ontong Java Plateau (Fornaciari et al., 1993). According to these studies, the common *S. capricornutus* and *S. delphix* in Sample 184-1148-48X-4, 81–82 cm, suggest that at least the upper part of Zone NN1 is preserved at Site 1148.

Above Core 184-1148-48X, the FO of *D. druggii*, a marker for the NN2/NN1 zonal boundary, was difficult to identify in samples between 405.7 and 458.7 mcd from Core 184-1148A-47X because of heavy overgrowth of *Discoaster* species in this interval. *D. druggii* and other discoasters are overgrown, showing thick and wide rays and making identification difficult. After a careful examination, a few moderately preserved *D. druggii* were observed at 454.35 mcd, assigning the lowest occurrence of this species (23.2 Ma) at this level and defining the NN2/NN1 zonal boundary.

The Oligocene/Miocene boundary as defined by calcareous nannofossils is placed at the top of Zone NP25 by some authors and within Zone NN1 by others. According to Berggren et al. (1995), the age of the Oligocene/Miocene boundary is 23.80 Ma, placed within Zone NN1. The LO of *S. delphix*, with an age of 23.80 Ma, determined for Site 1148 allows us conveniently to place the Oligocene/Miocene boundary at the level of the LO of *S. delphix*, within Zone NN1 and between the depths of 457.82 and 458.57 mcd at Site 1148.

Miocene

Above the FO of *D. druggii*, the FO of *Sphenolithus belemnos* was only obtained at Site 1148, defining the NN2/NN3 and CN1/CN2 zonal boundaries (Fig. F3). The LO of *Triquetrorhabdulus carinatus* appears much lower than the FO of *S. belemnos* at Site 1148; thus, it is not suitable for marking the NN2/NN3 zonal boundary in the area studied (Table T2). Fornaciari et al. (1990) estimated an age of 19.8 Ma for this event; however, we were unable to estimate the age of the LO of this species due to the lack of detailed age control, for example magnetic events in this interval.

The first event found at both Sites 1148 and 1146 is the LO of *S. belemnos* (Fig. F3), which marks the NN3/NN4 and CN2/CN3 zonal boundaries (Berggren et al., 1995). *S. belemnos* was observed between Samples 184-1146A-63X-CC, 33–39 cm, and 35–42 cm (633.76–643.1 mcd), placing the bottom of Site 1146 in Zone NN3 (18.3–19.2 Ma).

Above the LO of *S. belemnos*, the events recognized from Site 1148 can be well correlated with the same events from Site 1146 (Fig. F3). All ages and depths of these events are given in detail in Tables T2 and T3.

The next event is the LO of *Helicosphaera ampliaperta*, found at both sites, marking the NN4/NN5 or CN3/CN4 zonal boundaries (Fig. F2). The LO of *Sphenolithus heteromorphus* is used to define the NN5/NN6 or CN4/CN5a zonal boundaries in this study (Fig. F2). Within the Zone NN6 interval, we recognized two other events (i.e., the LO of *Cycliscardolithus floridanus* and the FO of *T. rugosus*) in agreement with several previous records (Olafsson, 1989; Rio et al., 1990; Raffi and Flores, 1995).

Discoaster kugleri is rare but continuously present in a short interval in the middle Miocene sequences at Sites 1146 and 1148, allowing the recognition of its FO and LO and the definition of the NN6/NN7 zonal boundary and the CN5a/CN5b subzonal boundary (Figs. F2, F3). *Catin-*

aster coalitus appears commonly to abundantly in our samples studied, and its FO serves as a good marker for the NN7/NN8 or CN5/CN6 zonal boundaries (Fig. F3). The LO of *D. kugleri* was found at a middle stratigraphic level in Zone NN7 at Sites 1146 and 1148.

Discoaster hamatus appears first with a notable abundance in the lower part of the upper Miocene sediments at Sites 1148 and 1146, assigning the NN8/NN9 and CN6/CN7 zonal boundaries for these two sites (Fig. F3). Zone NN8 or CN6 is a very short interval of ~10 m at Site 1146 and 4 m at Site 1148, in agreement with other studies (Raffi and Flores, 1995). The LO of *D. hamatus* marks the NN9/NN10 and CN7/CN8 zonal boundaries (Fig. F3).

Okada and Bukry (1980) used the FO of *Catinaster calyculus* to subdivide the CN7 Zone into Subzones CN7a and CN7b. However, its FO appears slightly below the FO of *D. hamatus*, about 2 m lower, for example, at Site 1148 and 3 m at Site 1146 (Tables T2, T3). Similar observations were reported from the Indian Ocean and the South Atlantic, respectively (Thierstein, 1974; Rio et al., 1990). Berggren et al. (1995) pointed out that the relationship between the FO of *C. calyculus* and the FO of *D. hamatus* is still poorly understood. Therefore, we did not subdivide Zone CN7. In the interval of Zone NN9, *C. coalitus* disappears first and then *C. calyculus* also becomes extinct below the LO of *D. hamatus*.

The top of Zone NN10 was defined by the FO of *Discoaster quinqueramus* (Martini, 1971), whereas that of Zone CN7 was defined by the FO of *Discoaster berggrenii* or the FO of *Discoaster surculus* (Okada and Bukry, 1980). Recently, *D. quinqueramus* and *D. berggrenii* were considered as synonyms, or *D. berggrenii* as a variety of *D. quinqueramus* (Rio et al., 1990; Raffi and Flores, 1995; Berggren et al., 1995). In our study, *D. quinqueramus* and *D. berggrenii* were still identified as two species and their FOs were found in the same sample at a site—for example, at 401.1 mcd at Site 1146 and at 240.92 mcd at Site 1148 (Tables T2, T3). Therefore, the NN10/NN11 and CN8/CN9 zonal boundaries can surely be defined (Fig. F2). Bukry (1973) further subdivided Zone CN8 into Subzones CN8a and CN8b by the FO of *Discoaster neorectus* and/or by the FO of *Discoaster loeblichii*. These two species are easily identifiable without confusion (Perch-Nielsen, 1985). However, they appear down to Zone NN9 in our northern Sites 1146 and 1148 and in the southern Site 1143 of the SCS (Wang, Prell, Blum, et al., 2000). According to Xu (1996), the same case appears in sediments from the offshore basin of the SCS. The much earlier appearance of these two species made the subdivision of Zone CN8 impossible.

In our samples, *D. berggrenii* disappears slightly later than *D. quinqueramus*, suggesting a slight difference in their stratigraphic ranges. In this paper, we used the LO of *D. quinqueramus* to define the NN11/NN12 and CN9/CN10 zonal boundaries (Fig. F3). The FO of *Amaurolithus primus* was used to subdivide Zone NN11 into Subzones CN9a and CN9b, in line with the definition of Okada and Bukry (1980). The FO and LO of *Amaurolithus amplificus* appear within Zone NN11.

The FO of *Ceratolithus acutus* and the LO of *T. rugosus* were found at the same level within Zone NN12. We differentiated Subzones CN10a and CN10b, following Bukry (1973).

Pliocene

According to Berggren et al. (1995), the age of the Oligocene/Miocene boundary is 23.80 Ma (Fig. F2). Recent studies suggest an age of

5.34 Ma for the LO of *C. acutus*, which is located within Zone NN12 and marks the top of Subzone CN10a (Young et al., 1994; Berggren et al., 1995). The next event above it is the FO of *Ceratolithus rugosus* with an age of 5.07 Ma, defining the tops of Zone NN12 and Subzone CN10b.

Following Berggren et al. (1995), we placed the Miocene/Pliocene boundary between the LO of *C. acutus* and the FO of *C. rugosus* in the upper part of Zone NN12 or between Subzones CN10a and CN10b.

Above the FO of *C. rugosus*, determination of the FO of *D. asymmetricus* in the sequences was somewhat difficult; because five rayed discoasters in that interval are poorly preserved, most arms were broken or lost. The FO of *Discoaster asymmetricus* in this study was determined based on finding relatively complete specimens. *C. acutus* becomes extinct somewhat earlier than the FO of *D. asymmetricus*. The LO of *Amaurolithus tricorniculatus* or *Amaurolithus* spp. marks the tops of Zones NN14 and CN10 (Fig. F2).

In this study, *R. pseudoumbilicus* is identified for specimens having a maximum coccolith length $>7\ \mu\text{m}$, in accord with Gartner (1967). The LO of *Sphenolithus abies/neoabies* appears shortly after the LO of *R. pseudoumbilicus*; the interval between these two events is $\sim 1\ \text{m}$ at Site 1146 and 3 m at Site 1148 (Tables T2, T3)

The LO of *D. surculus* is easily recognizable in the sections studied, and it was used to mark the NN16/NN17 and CN12/CN13 zonal boundaries (Fig. F2). The LO of *D. tamalis* was found in the relatively long interval of Zone NN16 in the Pliocene, subdividing this interval into Subzones CN12a and CN12b.

The tops of Zone NN17 and Subzone CN12c were defined by the LO of *Discoaster pentaradiatus* (Fig. F2). Zone NN17 is very thin at these two sites, $\sim 10\ \text{m}$, in agreement with the record of this zone in other areas.

Reworking of discoasters is very common in the upper sections at Sites 1146 and 1148, causing difficulty in determining the LO of *D. brouweri*. The event was determined by its appearance with reasonable abundance.

The Pliocene/Pleistocene boundary as defined by calcareous nannofossils is usually set above the LO of *D. brouweri*. The appearance of larger species of *Gephyrocapsa* gives an indication of the younger age of the sediment (Perch-Nielsen, 1985). In our study, the Pleistocene/Pliocene boundary is constrained by the FO of *Gephyrocapsa* (medium) spp. and the LO of *D. brouweri* and is located between 1.69 and 1.96 Ma.

Pleistocene

The lowermost Pleistocene Zone NN19 was defined from the LO of *D. brouweri* to the LO of *Pseudoemiliania lacunosa*. The LO of *Calcidiscus macintyreii* and the FO and LO of *R. asanoi* were recognized within this interval. *H. sellii* is rarely and sporadically present in the Pliocene and lower Pleistocene sequences at Sites 1148 and 1146 in the northern SCS and also at Site 1143 in the southern SCS (Wang, Prell, Blum, et al., 2000); thus, its LO is not determinable in this study.

Okada and Bukry (1980) used the FO of *Gephyrocapsa carribeanica* and the FO of *Gephyrocapsa oceanica* to subdivide the interval of Zone NN19 into Subzones CN13a, CN13b, and CN14a. As discussed in the taxonomic notes in this paper, there are morphological intergradients between different *Gephyrocapsa* species and a detailed study is needed to find reliable and applicable criteria to separate them. Thus, in the present study, we did not make a further subdivision for this interval.

The interval characterized by absences of *P. lacunosa* and *E. huxleyi* but by abundant *Gephyrocapsa oceanica* was defined as Zone NN20 and Subzone CN14b (Fig. F2). The FO of *E. huxleyi* was determined both by means of light microscope and scanning electron microscope and marks the bases of Zones NN21 and CN15. Gartner (1977) suggested this to be the acme of *E. huxleyi*. The determination of the acme of *E. huxleyi* was based upon a semiquantitative method.

Variation in Sedimentation Rates and Unconformity

The ages of these events were plotted against their depths to show variation in average linear sedimentation rates (Fig. F6). Sedimentation rates at Site 1146 are higher than those at Site 1148, most likely a result of having more terrestrial supplies due to its location closer to shore than Site 1148. Both sites show the same trend of downcore variation in sedimentation rates.

A very high sedimentation rate (35.6 cm/k.y.) was seen in the Oligocene section at Site 1148 and is probably a result of seafloor spreading (Wang, Prell, Blum, et al., 2000).

A significant unconformity was seen in the transition from upper Oligocene to lower Miocene. The nannofossil record indicated the absence of the uppermost part of Oligocene Zone NP25 and the lower part of Miocene Zone NN1. The time span of the unconformity was estimated to be ~1 m.y. based on the LO of *S. ciproensis* (24.75 Ma) in the upper part of Zone NP25 and the LOs of *S. capricornutus* and *S. delphix* (23.7 and 23.8 Ma) in the upper part of Zone NN1. The sedimentation rate is only ~3 cm/k.y. in this interval. The sedimentation rate in the interval between the LOs of *S. delphix* and *S. distentus* (27.5 Ma) is also very low—only 5 cm/k.y.

Sedimentation rates increase since the early Miocene and reach the highest values in Pleistocene—for example, from 14.5 to 22 cm/k.y. and to 64.6 cm/k.y. at Site 1148, although it reaches to 105 cm/k.y. in the Pleistocene at Site 1146. This agrees with Wang, Prell, Blum, et al. (2000), who found Miocene sediments rich in carbonate in conjunction with a general increase of noncarbonate sediment accumulation after 2–3 m.y. and a more significant increase in the latter part of the last million years.

CONCLUSION

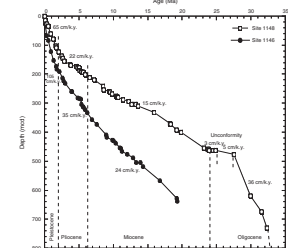
A total of 53 nannofossil events were recognized in the lower Oligocene to Pleistocene sediments studied. The sediments at the base of Site 1148 are in the lowermost lower Oligocene Zone NP22 with an age younger than 32.8 Ma.

Based on these events, the lower Oligocene to Pleistocene sequences recovered at Sites 1146 and 1148 were subdivided into the 4 Paleogene zones and 21 Neogene to Quaternary zones of Martini (1971), in correlation with the 3 Paleogene zones and 15 Neogene to Quaternary zones of Okada and Bukry (1980).

A significant unconformity was recognized in the Oligocene–Miocene transition, in which the upper part of Oligocene Zone NP25 and the lower part of Miocene Zone NN1 were missing. The time span of the unconformity was estimated to be ~1 m.y.

Very high sedimentation rates were seen in the Oligocene, along with relatively low values in the Miocene and the highest in the Pleis-

F6. Downcore variation in sedimentation rates, p. 21.



tocene; these rates were seen as the result of tectonic and sedimentation history of the SCS.

ACKNOWLEDGMENTS

This research used samples and data provided by the Ocean Drilling Program (ODP). ODP is sponsored by the U.S. National Science Foundation (NSF) and participating countries under management of Joint Oceanographic Institutions (JOI), Inc. Our heartfelt thanks go to the *JOIDES Resolution* crew, the SEDCO drilling crew, and the ODP technical crew for their enthusiastic cooperation and support. The success of this cruise is a tribute to Co-Chief Scientists Pinxian Wang and Warren Prell and Staff Scientist Peter Blum. Suggestions from Peter Blum and other reviewers improved the manuscript. This study was supported by the China Natural Sciences Foundation (grant no. 49732060).

REFERENCES

- Backman, J., 1980. Miocene–Pliocene nannofossils and sedimentation rates in the Hatton-Rockall Basin, NE Atlantic Ocean. *Stockholm Contrib. Geol.*, 36:1–91.
- Backman, J., and Hermelin, J.O.R., 1986. Morphometry of the Eocene nannofossil *Reticulofenestra umbilicus* lineage and its biochronological consequences. *Palaeogeogr., Palaeoclimatol., Palaeoecol.*, 57:103–116.
- Backman, J., and Raffi, I., 1997. Calibration of Miocene nannofossil events to orbitally tuned cyclostratigraphies from Ceara Rise. In Shackleton, N.J., Curry, W.B., Richter, C., and Bralower, T.J. (Eds.), *Proc. ODP, Sci. Results*, 154: College Station, TX (Ocean Drilling Program), 83–99.
- Backman, J., Schneider, D.A., Rio, D., and Okada, H., 1990. Neogene low-latitude magnetostratigraphy from Site 710 and revised age estimates of Miocene nannofossil datum events. In Duncan, R.A., Backman, J., Peterson, L.C., et al., *Proc. ODP, Sci. Results*, 115: College Station, TX (Ocean Drilling Program), 271–276.
- Backman, J., and Shackleton, N.J., 1983. Quantitative biochronology of Pliocene and early Pleistocene calcareous nannofossils from the Atlantic, Indian and Pacific oceans. *Mar. Micropaleontol.*, 8:141–170.
- Berggren, W.A., Kent, D.V., Swisher, C.C., III, and Aubry, M.-P., 1995. A revised Cenozoic geochronology and chronostratigraphy. In Berggren, W.A., Kent, D.V., Aubry, M.-P., and Hardenbol, J. (Eds.), *Geochronology, Time Scales and Global Stratigraphic Correlation*. Spec. Publ.—SEPM (Soc. Sediment. Geol.), 54:129–212.
- Bukry, D., 1973. Low-latitude coccolith biostratigraphic zonation. In Edgar, N.T., Saunders, J.B., et al., *Init. Repts. DSDP*, 15: Washington (U.S. Govt. Printing Office), 685–703.
- Bukry, D., 1975. Coccolith and silicoflagellate stratigraphy, northwestern Pacific Ocean, Deep Sea Drilling Project Leg 32. In Larson, R.L., Moberly, R., et al., *Init. Repts. DSDP*, 32: Washington (U.S. Govt. Printing Office), 677–701.
- Cande, S.C., and Kent, D.V., 1992. A new geomagnetic polarity time scale for the Late Cretaceous and Cenozoic. *J. Geophys. Res.*, 97:13917–13951.
- Cande, S.C., and Kent, D.V., 1995. Revised calibration of the geomagnetic polarity timescale for the Late Cretaceous and Cenozoic. *J. Geophys. Res.*, 100:6093–6095.
- Curry, W.B., Shackleton, N.J., Richter, C., et al., 1995. *Proc. ODP, Init. Repts*, 154: College Station, TX (Ocean Drilling Program).
- Duan, W., 1985. Calcareous nannofossils from two deep-sea cores in the northern South China Sea. *Acta Micropaleontol. Sinica*, 2:92–103. (in Chinese, with English abstract)
- Duan, W., and Huang, Y., 1991. Tertiary calcareous nannofossil biostratigraphy in the north part of the South China Sea. *Dizhi Xuebao*, 4:331–338. (in Chinese, with English abstract)
- Fornaciari, E., Backman, J., and Rio, D., 1993. Quantitative distribution patterns of selected lower to middle Miocene calcareous nannofossils from the Ontong Java Plateau. In Berger, W.H., Kroenke, L.W., Mayer, L.A., et al., *Proc. ODP, Sci. Results*, 130: College Station, TX (Ocean Drilling Program), 245–256.
- Fornaciari, E., Raffi, I., Rio, D., Villa, G., Backman, J., and Olafsson, G., 1990. Quantitative distribution patterns of Oligocene and Miocene calcareous nannofossils from the western equatorial Indian Ocean. In Duncan, R.A., Backman, J., Peterson, L.C., et al., *Proc. ODP, Sci. Results*, 115: College Station, TX (Ocean Drilling Program), 237–254.
- Gallagher, L., 1989. *Reticulofenestra*: a critical review of taxonomy, structure and evolution. In Crux, J.A., and van Heck, S.E. (Eds.), *Nannofossils and Their Applications*: Chichester (Ellis Horwood), 41–75.
- Gartner, S., 1967. Calcareous nannofossils from Neogene of Trinidad, Jamaica, and Gulf of Mexico. *Univ. Kansas Paleontol. Contrib.*, 29:1–7.

- Gartner, S., 1977. Calcareous nannofossil biostratigraphy and revised zonation of the Pleistocene. *Mar. Micropaleontol.*, 2:1–25.
- Gersonde, R., Hodell, D.A., Blum, P., et al., 1999. *Proc. ODP, Init. Repts.*, 177 [CD-ROM]. Available from: Ocean Drilling Program, Texas A&M University, College Station, TX 77845-9547, U.S.A.
- Huang, L., 1997. Calcareous nannofossil biostratigraphy in the Pearl River Mouth Basin, South China Sea, and Neogene reticulofenestrid coccoliths size distribution pattern. *Mar. Micropaleontol.*, 32:31–57.
- Huang, L., and Zhong, B., 1992. Calcareous nannofossil bioevents in the Oligocene–Pleistocene of the Pearl River Mouth Basin. *Shiyou Xuebao*, 13:169–177. (in Chinese, with English abstract)
- Martini, E., 1971. Standard Tertiary and Quaternary calcareous nannoplankton zonation. In Farinacci, A. (Ed.), *Proc. 2nd Int. Conf. Planktonic Microfossils Roma*: Rome (Ed. Tecnosci.), 2:739–785.
- Martini, E., and Müller, C., 1986. Current Tertiary and Quaternary calcareous nannoplankton stratigraphy and correlations. *Newsl. Stratigr.*, 16:99–112.
- Moran, M.J., and Watkins, D.K., 1988. Oligocene calcareous-nannofossil biostratigraphy from Leg 101, Site 628, Little Bahama Bank Slope. In Austin, J.A., Jr., Schlager, W., et al., *Proc. ODP, Sci. Results*, 101: College Station, TX (Ocean Drilling Program), 87–103.
- Okada, H., 1990. Quaternary and Paleogene calcareous nannofossils, Leg 115. In Duncan, R.A., Backman, J., Peterson, L.C., et al., *Proc. ODP, Sci. Results*, 115: College Station, TX (Ocean Drilling Program), 129–174.
- Okada, H., and Bukry, D., 1980. Supplementary modification and introduction of code numbers to the low-latitude coccolith biostratigraphic zonation (Bukry, 1973; 1975). *Mar. Micropaleontol.*, 5:321–325.
- Olafsson, G., 1989. Quantitative calcareous nannofossil biostratigraphy of upper Oligocene to middle Miocene sediment from ODP Hole 667A and middle Miocene sediment from DSDP Site 574. In Ruddiman, W., Sarnthein, M., et al., *Proc. ODP, Sci. Results*, 108: College Station, TX (Ocean Drilling Program), 9–22.
- Perch-Nielsen, K., 1985. Mesozoic calcareous nannofossils. In Bolli, H.M., Saunders, J.B., and Perch-Nielsen, K. (Eds.), *Plankton Stratigraphy*: Cambridge (Cambridge Univ. Press), 329–426.
- Poore, R.Z., Tauxe, L., Percival, S.F., Jr., and Labecoque, J.L., 1982. Late Eocene-Oligocene magnetostratigraphy and biostratigraphy at South Atlantic DSDP Site 522. *Geology*, 10:508–511.
- Raffi, I., and Flores, J.-A., 1995. Pleistocene through Miocene calcareous nannofossils from eastern equatorial Pacific Ocean. In Pisias, N.G., Mayer, L.A., Janecek, T.R., Palmer-Julson, A., and van Andel, T.H. (Eds.), *Proc. ODP, Sci. Results*, 138: College Station, TX (Ocean Drilling Program), 233–286.
- Rio, D., Fornaciari, E., and Raffi, I., 1990. Late Oligocene through early Pleistocene calcareous nannofossils from western equatorial Indian Ocean (Leg 115). In Duncan, R.A., Backman, J., Peterson, L.C., et al., *Proc. ODP, Sci. Results*, 115: College Station, TX (Ocean Drilling Program), 175–235.
- Sato, T., and Takayama, T., 1992. A stratigraphically significant new species of the calcareous nannofossil *Reticulofenestra asanoi*. In Ishizaki, K., and Saito, T. (Eds.), *Centenary of Japanese Micropaleontology*: Tokyo (Terra Sci. Publ.), 457–460.
- Shipboard Scientific Party, 2002. Site 1201. In Salisbury, M.H., Shinohara, M., Richter, C., et al., *Proc. ODP, Init. Repts.*, 195, 1–233 [CD-ROM]. Available from: Ocean Drilling Program, Texas A&M University, College Station TX 77845-9547, USA.
- Shyu, J.-P., and Müller, C.M., 1991. Calcareous nannofossil biostratigraphy of the Celebes and Sulu seas. In Silver, E.A., Rangin, C., von Breymann, M.T., et al., *Proc. ODP, Sci. Results*, 124: College Station, TX (Ocean Drilling Program), 133–158.
- Su, X., 1989. Calcareous nannoflora. In Hao, Y., et al., *Quaternary Microbiotas and Their Geological Significance from Northern Xisha Trench of South China Sea*: Beijing (China Univ. Geosci. Press), 52–57. (in Chinese, with English abstract)

- Su, X., 1996. Development of late Tertiary and Quaternary coccolith assemblages in the northeast Atlantic. *GEOMAR Rep.*, 48.
- Thierstein, H.R., 1974. Calcareous nannoplankton, Leg 26, Deep Sea Drilling Project. In Davies, T.A., Luyendyk, B.P., et al., *Init. Repts. DSDP, 26*: Washington (U.S. Govt. Printing Office), 619–667.
- Wang, P., Prell, W.L., Blum, P., et al., 2000. *Proc. ODP, Init. Repts.*, 184 [CD-ROM]. Available from: Ocean Drilling Program, Texas A&M University, College Station TX 77845-9547, USA.
- Wei, W., 1992. Paleogene chronology of Southern Ocean drill holes: an update. In Kennett, J.P., and Warnke, D.A. (Eds.), *The Antarctic Paleoenvironment: A Perspective on Global Change*. Antarct. Res. Ser., 56:75–96.
- Wei, W., and Thierstein, H.R., 1991. Upper Cretaceous and Cenozoic calcareous nanofossils of the Kerguelen Plateau (southern Indian Ocean) and Prydz Bay (East Antarctica). In Barron, J., Larsen, B., et al., *Proc. ODP, Sci. Results*, 119: College Station, TX (Ocean Drilling Program), 467–494.
- Wei, W., and Wise, S.W., Jr., 1989. Paleogene calcareous nanofossil magnetobiochronology: results from South Atlantic DSDP Site 516. *Mar. Micropaleontol.*, 14:119–152.
- Xu, Y., 1996. Tertiary calcareous nanofossil zones and paleoceanic environments of Pearl River Mouth Basin. In Hao, Y., et al., *Research on Micropaleontology and Paleooceanography in the Pearl River Mouth Basin, South China Sea*: Beijing (China Univ. Geosci. Press), 85–96. (in Chinese, with English abstract)
- Young, J.R., 1990. Size variation of Neogene *Reticulofenestra* coccoliths from Indian Ocean DSDP cores. *J. Micropaleontol.*, 9:71–85.
- Young, J.R., and Wei, W., et al., 1994. A summary chart of Neogene nanofossil magnetobiostratigraphy. *J. Nannoplankton Res.*, 16:21–27.

Figure F1. Location of ODP Sites 1146, 1147, and 1148 in the northern South China Sea (SCS). Thin lines with numbers are water depth (m).

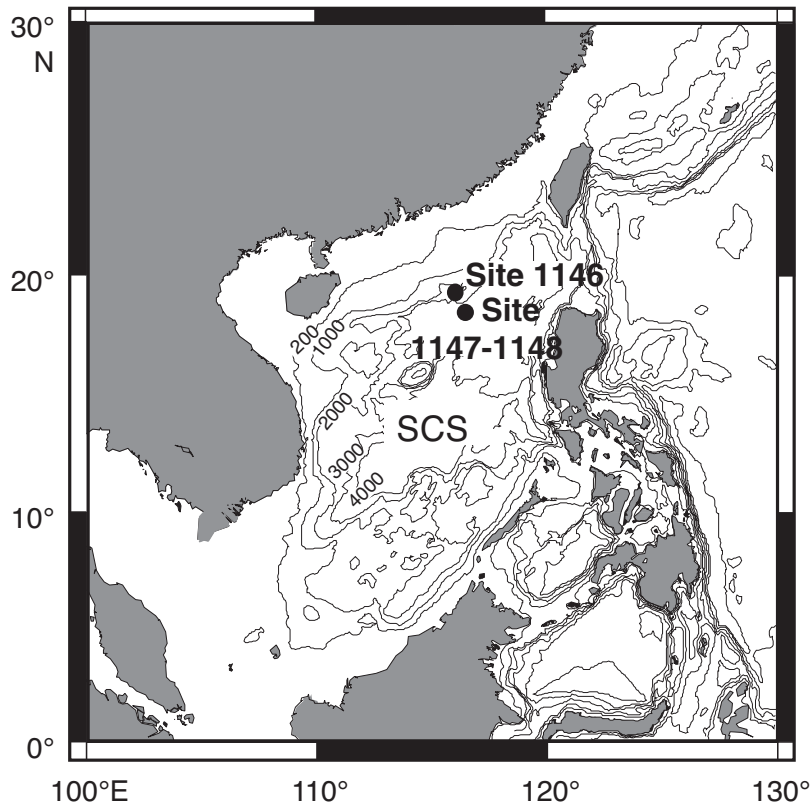


Figure F2. Chronostratigraphy and calcareous nannofossil biostratigraphic zonation. MPTS = magnetic polarity timescale, FO = first occurrence, LO = last occurrence. (Continued on next page.)

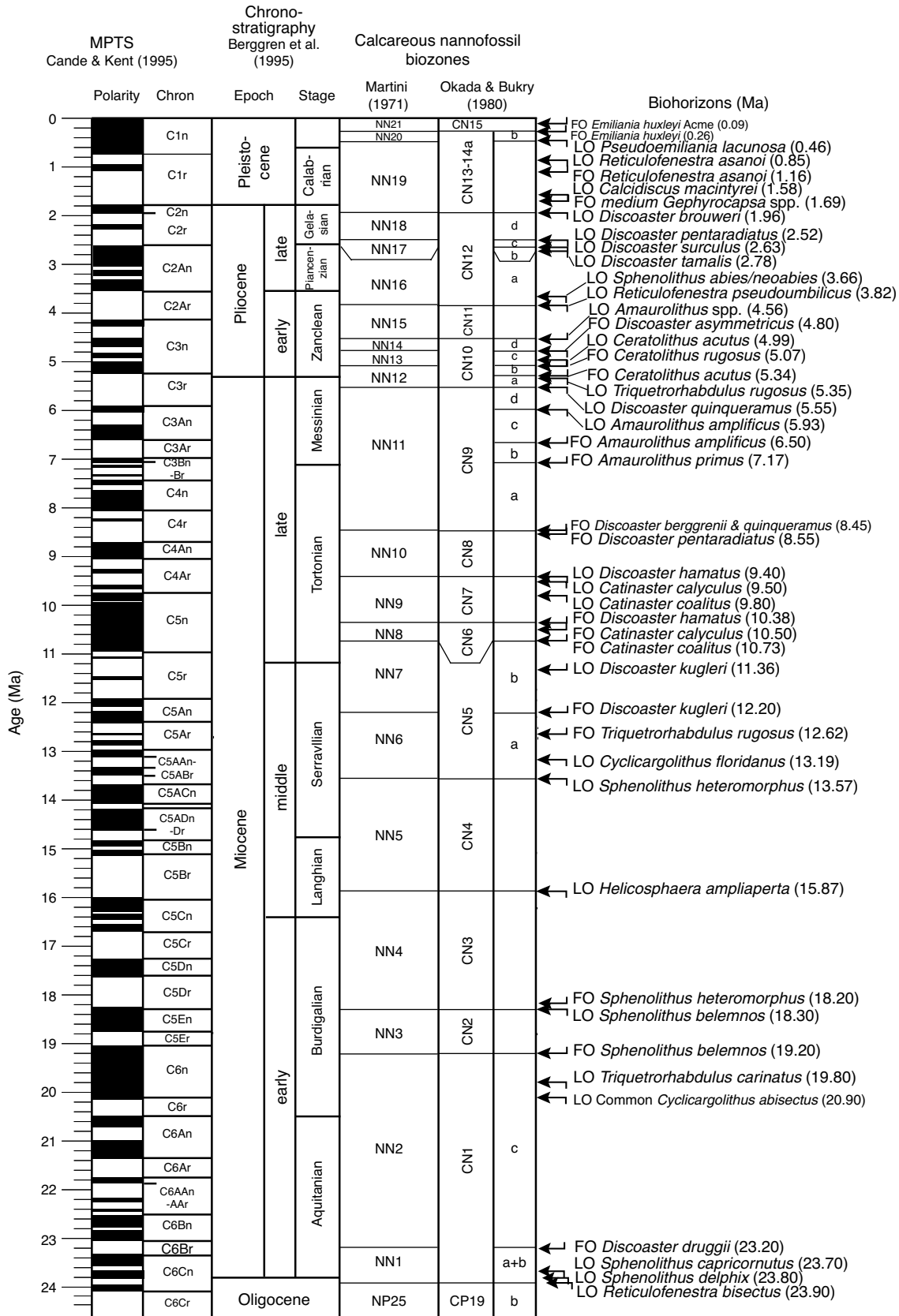


Figure F2 (continued).

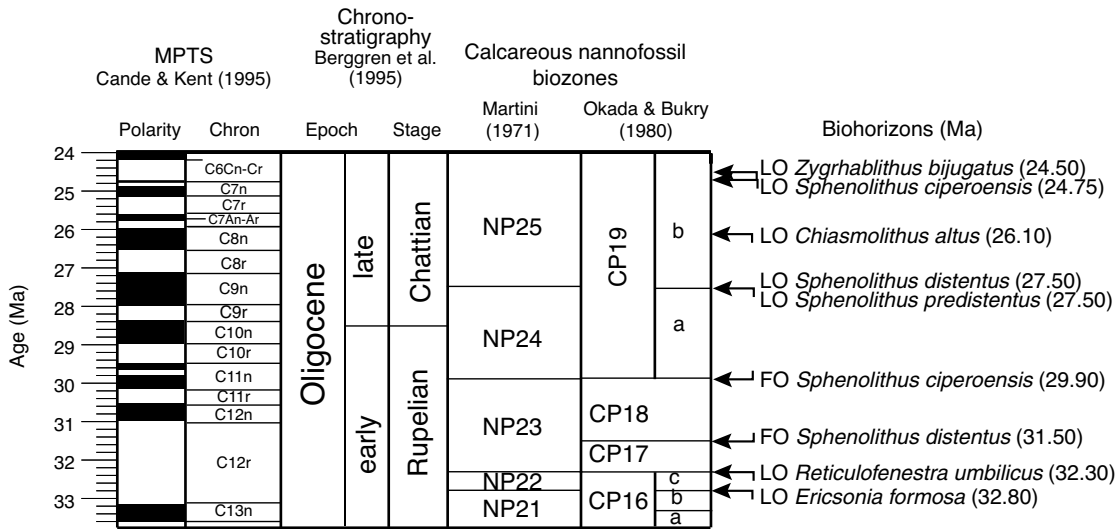


Figure F3. Correlation of calcareous nannofossil zones at Sites 1148 and 1146. FO = first occurrence, LO = last occurrence.

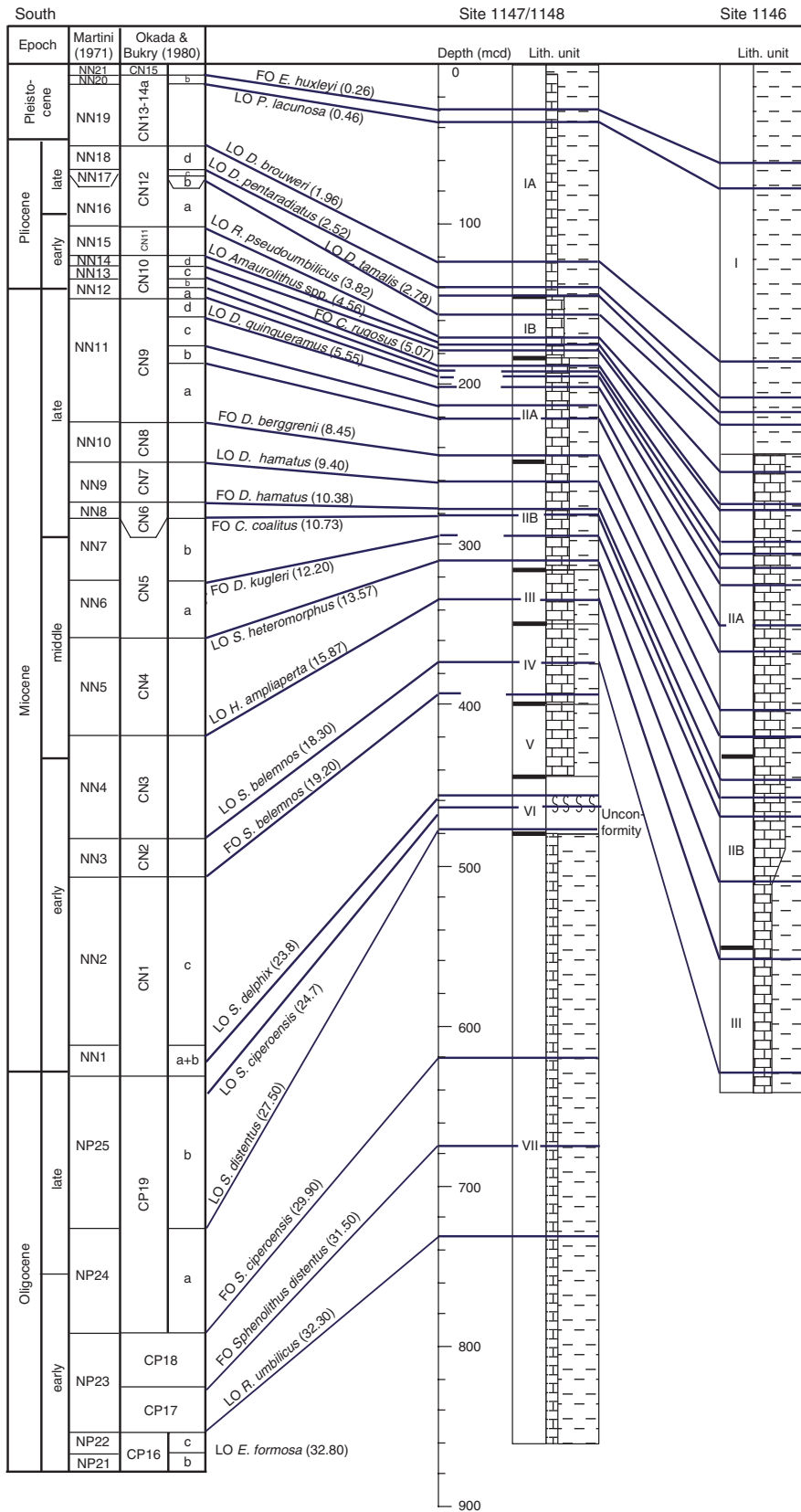


Figure F4. Variation in abundance of several marker species around the NP25/NN1 boundary. LO = last occurrence.

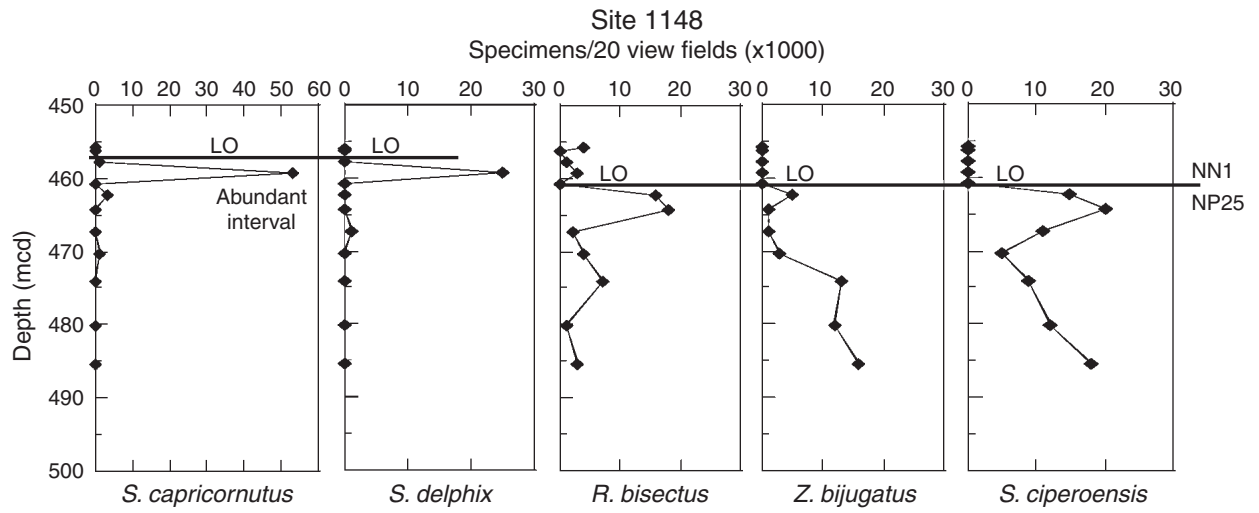


Figure F5. Appearance of several marker species around the Oligocene/Miocene boundary. The range of fossils is plotted against original “mbsf” in Hole 1148A. The lithologic log is after core description by Wang, Prell, Blum, et al. (2000).

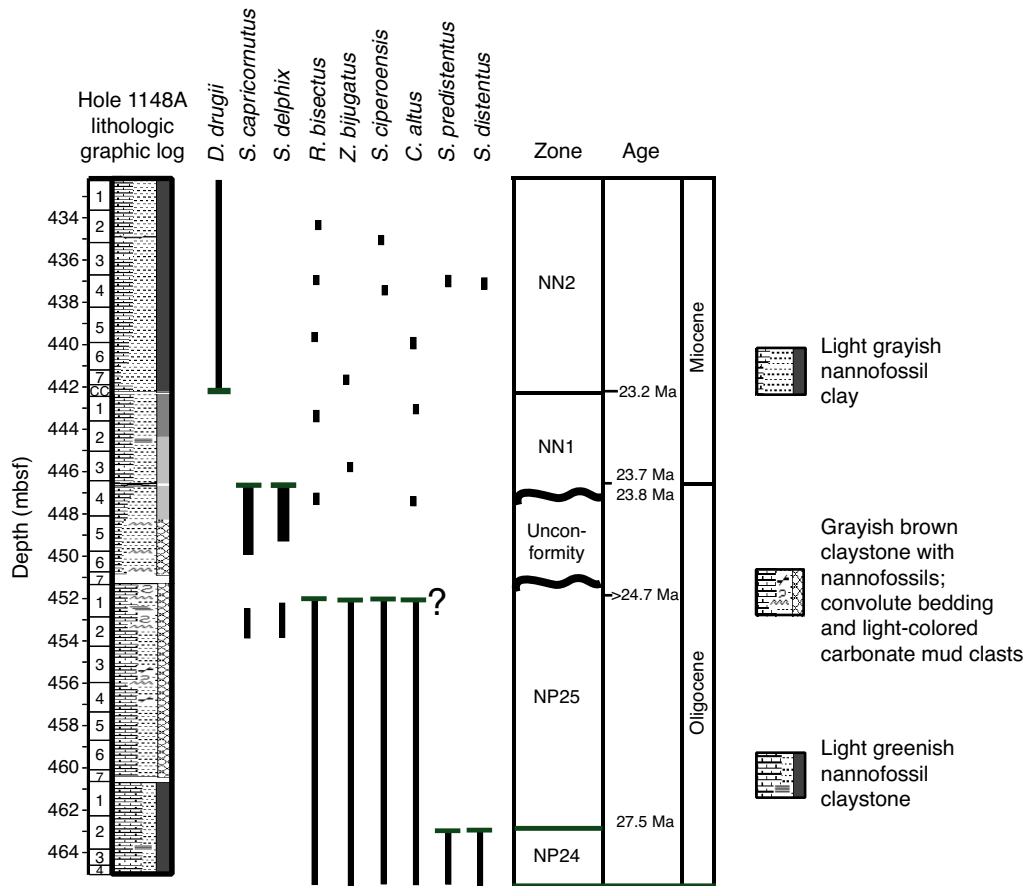


Figure F6. Downcore variation in sedimentation rates for Sites 1148 and 1146.

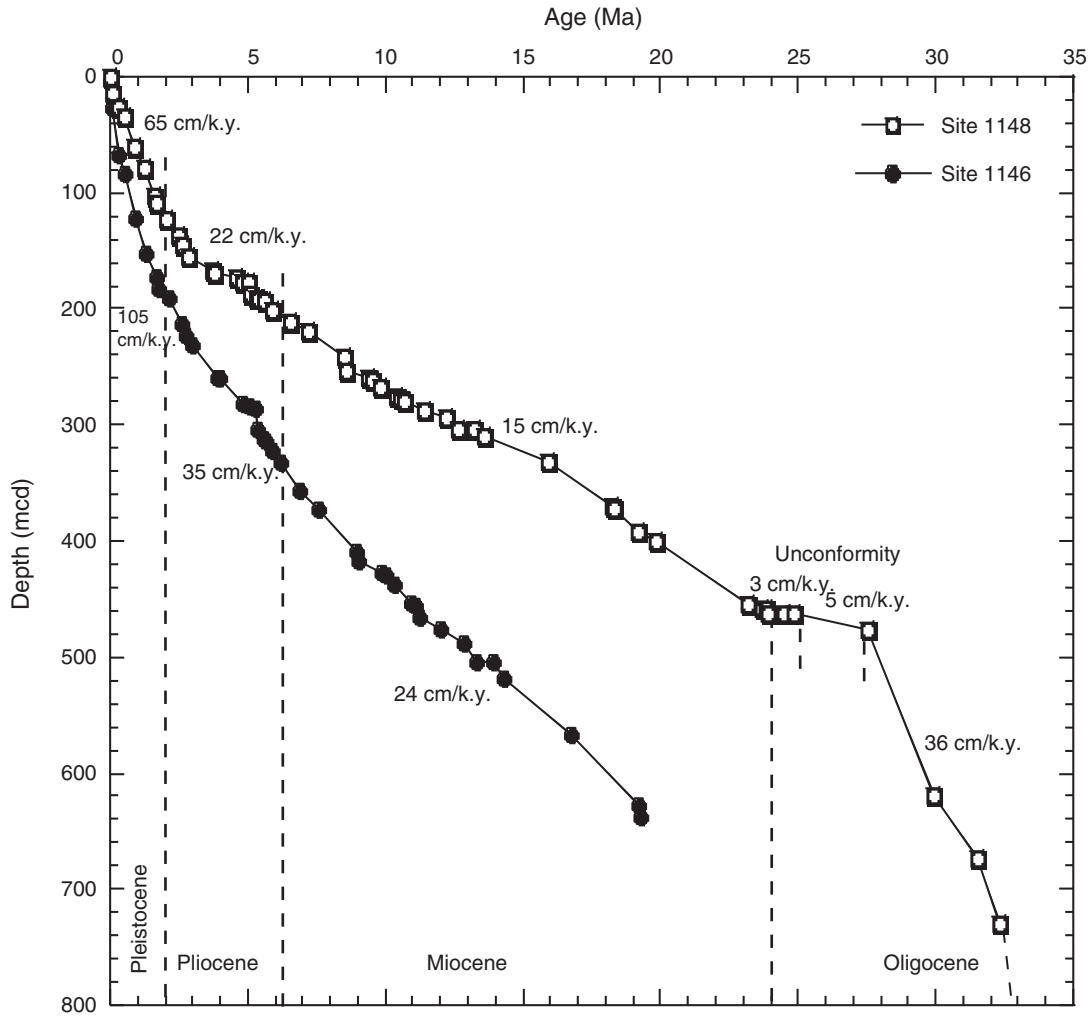


Table T1. Location of ODP Sites 1146, 1147, and 1148.

Site	Latitude	Longitude	Water depth (m)	Cored interval (mbsf)	Age interval
1146	116°16.37'E	19°27.40'N	2092	0–606.66	Pleistocene–Miocene
1147	116°33.28'E	18°50.11'N	3246	0–76.60	Pleistocene
1148	116°33.93'E	18°50.17'N	3294	0–845.10	Pleistocene–Oligocene

Table T2. Depths and ages of calcareous nannofossil events at Site 1148.

Event	Age (Ma)	Reference	Interval							Mean depth (mcd)
			Top			Bottom				
			Hole	Core, section, interval (cm)	Depth (mcd)	Hole	Core, section, interval (cm)	Depth (mcd)		
FO <i>E. huxleyi</i> Acme	0.09	1	1147B	2H-2, 80–81	12.30	1147B	2H-3, 80–81	13.80	13.05	
FO <i>E. huxleyi</i>	0.26	2	1147C	4H-2, 80–81	25.95	1147A	3H-CC, 16–22	26.39	26.17	
LO <i>P. lacunosa</i>	0.46	2	1148A	4H-CC, 30–37	34.35	1147B	4H-4, 80–81	35.50	34.93	
LO <i>R. asanoi</i>	0.85	1	1148A	7H-3, 80–81	59.00	1148A	7H-4, 80–81	60.50	59.75	
FO <i>R. asanoi</i>	1.16	1	1148B	8H-5, 80–81	77.62	1148A	9H-3, 80–81	78.77	78.20	
LO <i>C. macintyreii</i>	1.58	2	1148A	11H-5, 80–81	101.82	1148B	11H-2, 80–81	103.22	102.52	
FO <i>Gephyrocapsa</i> (medium) spp.	1.69	2	1148B	11H-6, 80–81	109.22	1148A	12H-3, 80–81	109.27	109.25	
LO <i>D. brouweri</i>	1.96	2	1148A	13H-4, 80–81	121.70	1148A	13H-5, 80–81	122.95	122.33	
LO <i>D. pentaradiatus</i>	2.52	2	1148B	14H-4, 80–81	136.60	1148B	14H-4, 80–81	136.60	136.60	
LO <i>D. surculus</i>	2.63	2	1148B	15H-2, 80–81	144.15	1148A	15H-6, 80–81	144.60	144.38	
LO <i>D. tamalis</i>	2.78	2	1148A	16H-6, 80–81	154.32	1148A	16H-CC, 0–8	155.44	154.88	
LO <i>S. abies/neoabies</i>	3.66	2	1148A	18H-1, 80–81	165.92	1148A	18H-2, 80–81	167.42	166.67	
LO <i>R. pseudoumbilicus</i>	3.82	2	1148A	18H-3, 80–81	168.92	1148A	18H-4, 80–81	170.42	169.67	
LO <i>Amaurolithus</i> spp.	4.56	2	1148A	18H-5, 80–81	171.92	1148A	18H-CC, 44–51	173.76	172.84	
FO <i>D. asymmetricus</i>	4.80	4	1148A	19H-1, 80–81	175.52	1148A	19H-2, 80–81	177.02	176.27	
LO <i>C. acutus</i>	4.99	2	1148A	19H-2, 80–81	177.02	1148A	19H-3, 80–81	178.52	177.77	
FO <i>C. rugosus</i>	5.07	2	1148A	20H-2, 80–81	186.62	1148A	20H-3, 80–81	188.12	187.37	
FO <i>C. acutus</i>	5.34	2	1148A	20H-4, 80–81	189.62	1148A	20H-5, 80–81	191.12	190.37	
LO <i>T. rugosus</i>	5.35	2	1148A	20H-5, 80–81	191.12	1148A	20H-6, 80–81	192.62	191.87	
LO <i>D. quinqueramus</i>	5.55	2	1148A	20H-6, 80–81	192.62	1148A	20H-CC, 0–7	193.75	193.19	
LO <i>A. amplificus</i>	5.93	2	1148A	21H-4, 80–81	199.32	1148A	21H-5, 80–81	200.82	200.07	
FO <i>A. amplificus</i>	6.50	2	1148A	22H-5, 80–81	210.52	1148A	22H-6, 80–81	212.02	211.27	
FO <i>A. primus</i>	7.17	2	1148A	23H-4, 80–81	218.62	1148A	23H-5, 80–81	220.12	219.37	
FO <i>D. berggrenii</i>	8.45	2	1148A	25H-6, 80–81	240.92	1148A	25H-CC, 32–39	242.41	241.67	
FO <i>D. quinqueramus</i>	8.45	2	1148A	25H-6, 80–81	240.92	1148A	25H-CC, 32–39	242.41	241.67	
FO <i>D. pentaradiatus</i>	8.55	2	1148A	27H-1, 80–81	252.62	1148A	27H-2, 80–81	254.12	253.37	
LO <i>D. hamatus</i>	9.40	2	1148A	27H-5, 80–81	258.62	1148A	27H-6, 80–81	260.12	259.37	
LO <i>C. calyculus</i>	9.50	4	1148A	27H-CC, 45–52	261.66	1148A	28H-1, 80–81	262.22	261.94	
LO <i>C. coalitus</i>	9.80	4	1148A	28H-4, 80–81	266.72	1148A	28H-5, 80–81	268.22	267.47	
FO <i>D. hamatus</i>	10.38	2	1148A	29H-3, 80–81	274.82	1148A	29H-4, 80–81	276.32	275.57	
FO <i>C. calyculus</i>	10.50	4	1148A	29H-4, 80–81	276.32	1148A	29H-5, 80–81	277.82	277.07	
FO <i>C. coalitus</i>	10.73	2	1148A	29H-CC, 26–33	279.46	1148A	30H-1, 80–81	281.42	280.44	
LO <i>D. kugleri</i>	11.36	2	1148A	30H-5, 80–81	287.42	1148A	30H-6, 80–81	288.92	288.17	
FO <i>D. kugleri</i>	12.20	2	1148A	31H-2, 80–81	292.52	1148A	31H-3, 80–81	294.02	293.27	
FO <i>T. rugosus</i>	12.62	2	1148A	32H-2, 80–81	302.12	1148A	32H-3, 80–81	303.62	302.87	
LO <i>C. floridanus</i>	13.19	2	1148A	32H-2, 80–81	302.12	1148A	32H-3, 80–81	303.62	302.87	
LO <i>S. heteromorphus</i>	13.57	2	1148A	32H-6, 80–81	308.12	1148A	32H-CC, 16–26	309.50	308.81	
LO <i>H. ampliiperta</i>	15.87	2	1148A	35H-2, 80–81	331.12	1148A	35H-3, 80–81	332.62	331.87	
FO <i>S. heteromorphus</i>	18.20	3	1148A	39H-2, 80–81	369.42	1148A	39H-3, 80–81	370.92	370.17	
LO <i>S. belemnos</i>	18.30	3	1148A	39H-4, 60–	372.22	1148A	39H-4, 80–81	372.42	372.32	
FO <i>S. belemnos</i>	19.20	3	1148A	41H-3, 80–81	390.22	1148A	41H-4, 80–81	391.72	390.97	
LO <i>T. carinatus</i>	19.80	3	1148A	42H-3, 80–81	399.92	1148A	42H-4, 80–81	401.42	400.67	
FO <i>D. druggii</i>	23.20	3	1148A	47H-CC, 41–48	454.35	1148A	48H-1, 80–81	454.82	454.59	
LO <i>S. capricornutus</i>	23.70	3	1148A	48H-3, 80–81	457.82	1148A	48H-4, 80–81	459.32	458.57	
LO <i>S. delphix</i>	23.80	3	1148A	48H-3, 80–81	457.82	1148A	48H-4, 80–81	459.32	458.57	
LO <i>R. bisectus</i>	23.90	3	1148A	48H-5, 80–81	460.82	1148A	48H-6, 80–81	462.32	461.57	
LO <i>Z. bijugatus</i>	24.50	3	1148A	48H-5, 80–81	460.82	1148A	48H-6, 80–81	462.32	461.57	
LO <i>S. ciperoensis</i>	24.75	3	1148A	48H-5, 80–81	460.82	1148A	48H-6, 80–81	462.32	461.57	
LO <i>S. distentus</i>	27.50	3	1148B	18H-CC, 38–45	474.85	1148A	50H-CC, 34–41	477.34	476.10	
LO <i>S. predistentus</i>	27.50	3	1148B	18H-CC, 38–45	474.85	1148A	50H-CC, 34–41	477.34	476.10	
FO <i>S. ciperoensis</i>	29.90	3	1148B	34H-CC, 26–33	617.16	1148A	67H-CC, 30–37	620.00	618.58	
FO <i>S. distentus</i>	31.50	3	1148A	73H-3, 77–78	671.89	1148A	73H-5, 80–81	674.92	673.41	
LO <i>R. umbilicus</i>	32.30	3	1148B	41H-3, 80–81	729.12	1148B	41H-5, 80–81	731.54	730.33	

Notes: 1 = Su (1996), 2 = Shackleton et al. (1995), 3 = Berggren et al. (1995), 4 = ages from various references. FO = first occurrence, LO = last occurrence.

Table T3. Depths and ages of calcareous nannofossil events at Site 1146.

Event	Age (Ma)	Reference	Interval						Mean depth (mcd)
			Top			Bottom			
			Hole	Core, section, interval (cm)	Depth (mcd)	Hole	Core, section, interval (cm)	Depth (mcd)	
FO <i>E. huxleyi</i> Acme	0.09	1	1146A	3H-CC, 13–20	23.10	1146B	3H-5, 1–2	22.81	22.96
FO <i>E. huxleyi</i>	0.26	2	1146B	7H-2, 81–82	61.11	1146B	7H-3, 41–42	62.21	61.66
LO <i>P. lacunosa</i>	0.46	2	1146C	8H-5, 61–62	77.56	1146C	8H-6, 61–62	79.06	78.31
LO <i>R. asanoi</i>	0.85	1	1146C	12H-4, 61–62	117.01	1146C	12H-5, 11–12	118.01	117.51
FO <i>R. asanoi</i>	1.16	1	1146A	15H-CC, 25–32	145.52	1146C	15H-3, 121–122	146.46	145.99
LO <i>C. macintyreii</i>	1.58	2	1146A	18H-1, 141–142	167.36	1146A	18H-2, 1–2	167.46	167.41
FO <i>Gephyrocapsa</i> spp. (medium)	1.69	2	1146B	18H-6, 41–42	176.96	1146B	18H-6, 141–142	177.96	177.46
LO <i>D. brouweri</i>	1.96	2	1146A	19H-CC, 20–26	185.46	1146C	19H-3, 11–12	185.51	185.49
LO <i>D. pentaradiatus</i>	2.52	2	1146C	21H-4, 41–42	207.86	1146C	21H-4, 51–52	207.96	207.91
LO <i>D. surculus</i>	2.63	2	1146B	22H-5, 71–72	217.36	1146B	22H-5, 81–82	217.46	217.41
LO <i>D. tamalis</i>	2.78	2	1146A	23H-5, 121–122	224.11	1146C	23H-2, 21–22	225.96	225.04
LO <i>S. abies/neoabies</i>	3.66	2	1146C	25H-6, 86–87	253.61	1146C	25H-6, 91–92	253.66	253.64
LO <i>R. pseudoumbilicus</i>	3.82	2	1146C	25H-6, 141–142	254.16	1146C	25H-6, 146–147	254.21	254.19
LO <i>Amaurolithus</i> spp.	4.56	2	1146C	27H-1, 136–137	274.10	1146A	28H-4, 146–147	274.90	274.50
FO <i>D. asymmetricus</i>	4.80	4	1146A	28H-5, 146–147	276.40	1146A	28H-CC, 16–23	278.09	277.25
LO <i>C. acutus</i>	4.99	2	1146A	29H-1, 81–83	279.81	1146C	28H-1, 71–72	281.06	280.44
FO <i>C. rugosus</i>	5.07	2	1146C	29H-6, 16–17	296.91	1146C	28H-1, 71–72	297.01	296.96
FO <i>C. acutus</i>	5.34	2	1146C	30H-5, 96–97	305.06	1146A	31H-CC, 23–30	306.29	305.68
LO <i>T. rugosus</i>	5.35	2	1146C	30H-6, 96–97	306.56	1146C	30H-7, 46–47	307.56	307.06
LO <i>D. quinqueramus</i>	5.55	2	1146A	32H-4, 15–16	313.90	1146A	32H-5, 15–16	315.40	314.65
LO <i>A. amplificus</i>	5.93	2	1146A	33H-5, 15–16	324.40	1146A	33H-CC, 15–32	325.77	325.09
FO <i>A. amplificus</i>	6.50	2	1146C	35H-4, 15–16	348.45	1146A	36H-2, 90–91	352.90	350.68
FO <i>A. primus</i>	7.17	2	1146A	37H-3, 90–91	364.75	1146A	37H-4, 90–91	366.25	365.50
FO <i>D. berggrenii</i>	8.45	2	1146C	40H-2, 90–91	401.16	1146C	40H-3, 90–91	402.66	401.91
FO <i>D. quinqueramus</i>	8.45	2	1146C	40H-2, 90–91	401.16	1146C	40H-3, 90–91	402.66	401.91
FO <i>D. pentaradiatus</i>	8.55	2	1146A	41H-5, 90–91	409.02	1146C	24H-35, 90–91	410.42	409.72
LO <i>D. hamatus</i>	9.40	2	1146C	42H-3, 15–16	419.12	1146A	42H-CC, 28–35	419.66	419.39
LO <i>C. calyculus</i>	9.50	4	1146C	42H-4, 15–16	420.62	1146A	43H-3, 15–16	423.32	421.97
LO <i>C. coalitus</i>	9.80	4	1146A	44H-1, 15–16	429.52	1146A	43H-CC, 33–40	429.53	429.53
FO <i>D. hamatus</i>	10.38	2	1146A	45H-5, 15–16	445.47	1146C	45H-2, 15–16	446.57	446.02
FO <i>C. calyculus</i>	10.50	4	1146C	45H-3, 15–16	448.07	1146C	45H-4, 15–16	449.57	448.82
FO <i>C. coalitus</i>	10.73	2	1146A	46H-5, 15–16	456.57	1146C	46H-2, 15–16	458.57	457.57
LO <i>D. kugleri</i>	11.36	2	1146A	47H-5, 15–16	468.17	1146A	47H-6, 15–16	469.67	468.92
FO <i>D. kugleri</i>	12.20	2	1146A	48H-5, 90–91	478.81	1146A	46H-CC, 37–42	479.97	479.39
FO <i>T. rugosus</i>	12.62	2	1146A	50H-5, 15–16	495.84	1146A	50H-6, 15–16	497.34	496.59
LO <i>C. floridanus</i>	13.19	2	1146A	50H-5, 15–16	495.84	1146A	50H-6, 15–16	497.34	496.59
LO <i>S. heteromorphus</i>	13.57	2	1146C	51H-4, 15–17	510.69	1146A	51H-CC, 32–39	510.87	510.78
LO <i>H. ampliapertura</i>	15.87	2	1146C	56H-2, 15–16	558.10	1146C	56H-3, 15–16	559.60	558.85
FO <i>S. heteromorphus</i>	18.20	3	1146A	61H-CC, 43–50	613.18	1146A	62H-CC, 19–26	623.03	618.11
LO <i>S. belemnus</i>	18.30	3	1146A	62H-CC, 19–26	623.03	1146A	63H-CC, 33–39	633.76	628.40

Notes: 1 = Su (1996), 2 = Shackleton et al. (1995), 3 = Berggren et al. (1995), 4 = ages from various references. FO = first occurrence, LO = last occurrence.